Hurricane Katrina (2005). Part I: Complex Life Cycle of an Intense Tropical Cyclone

RON MCTAGGART-COWAN AND LANCE F. BOSART

Department of Earth and Atmospheric Sciences, University at Albany, State University of New York, Albany, New York

JOHN R. GYAKUM AND EYAD H. ATALLAH

Department of Atmospheric and Oceanic Science, McGill University, Montreal, Quebec, Canada

(Manuscript received 5 May 2006, in final form 8 March 2007)

ABSTRACT

The devastating effects of Hurricane Katrina (2005) on the Gulf Coast of the United States are without compare for natural disasters in recent times in North America. With over 1800 dead and insured losses near $40 billion (U.S. dollars), Katrina ranks as the costliest and one of the deadliest Atlantic hurricanes in history. This study documents the complex life cycle of Katrina, a storm that was initiated by a tropical transition event in the Bahamas. Katrina intensified to a category-1 hurricane shortly before striking Miami, Florida; however, little weakening was observed as the system crossed the Florida peninsula. An analog climatology is used to show that this behavior is consistent with the historical record for storms crossing the southern extremity of the peninsula. Over the warm Gulf of Mexico waters, Katrina underwent two periods of rapid intensification associated with a warm core ring shed by the Loop Current. Between these spinup stages, the storm doubled in size, leading to a monotonic increase in power dissipation until Katrina reached a superintense state on 28 September. A pair of extremely destructive landfalls in Louisiana followed the weakening of the system over shelf waters. Despite its strength as a hurricane, Katrina did not reintensify following extratropical transition. The evolution of the storm's outflow anticyclone, however, led to a perturbation of the midlatitude flow that is shown in a companion study to influence the Northern Hemisphere over a period of 2 weeks. An understanding of the varied components of Katrina's complex evolution is necessary for further developing analysis and forecasting techniques as they apply to storms that form near the North American continent and rapidly intensify over the Gulf of Mexico. Given the observed overall increase in Atlantic hurricane activity since the mid-1990s, an enhanced appreciation for the forcings involved in such events could help to mitigate the impact of similar severe hurricanes in the future.

1. Introduction

Hurricane Katrina (August–September 2005) was both the deadliest and the costliest natural disaster to strike the United States in recent times. Its landfalls in Florida and Louisiana resulted in over 1800 deaths in Louisiana, Mississippi, Georgia, Alabama, and Florida (Knabb et al. 2005), and insured losses between $38 and $44 billion (U.S. dollars; Churney 2006). Clearly, an event of this magnitude is worthy of detailed study, especially given the increase in hurricane frequency that has been observed since the mid-1990s. The fragility of coastal infrastructure bordering the Gulf of Mexico has been demonstrated by the devastating effects of Katrina's well-forecasted landfall near New Orleans, Louisiana. An understanding of the forcings and mechanisms that lead to the development, movement, and rapid intensification of Hurricane Katrina is essential to further enhancing critical early warning systems in this high-risk environment predicted to experience at least a temporary overall increase in hurricane activity (Goldenberg et al. 2001; Emanuel 2005; Bell and Chelliah 2006).

Hurricane Katrina was first identified as Tropical Depression (TD) 12 by forecasters at the National Hurricane Center (NHC) at 1800 UTC 23 August 2005 over the southeastern Bahamas (Fig. 1). Moving initially northward, and then turning toward the west, the storm made landfall near Miami, Florida, shortly before 0000 UTC 26 August as category-1 (Simpson 1974) Hurricane Katrina with radar-estimated winds of 35 m s^{-1}

Corresponding author address: Ron McTaggart-Cowan, University at Albany, State University of New York, DEAS-ES351, Albany, NY 12222.
E-mail: rmctc@atmos.albany.edu

DOI: 10.1175/2007MWR1875.1

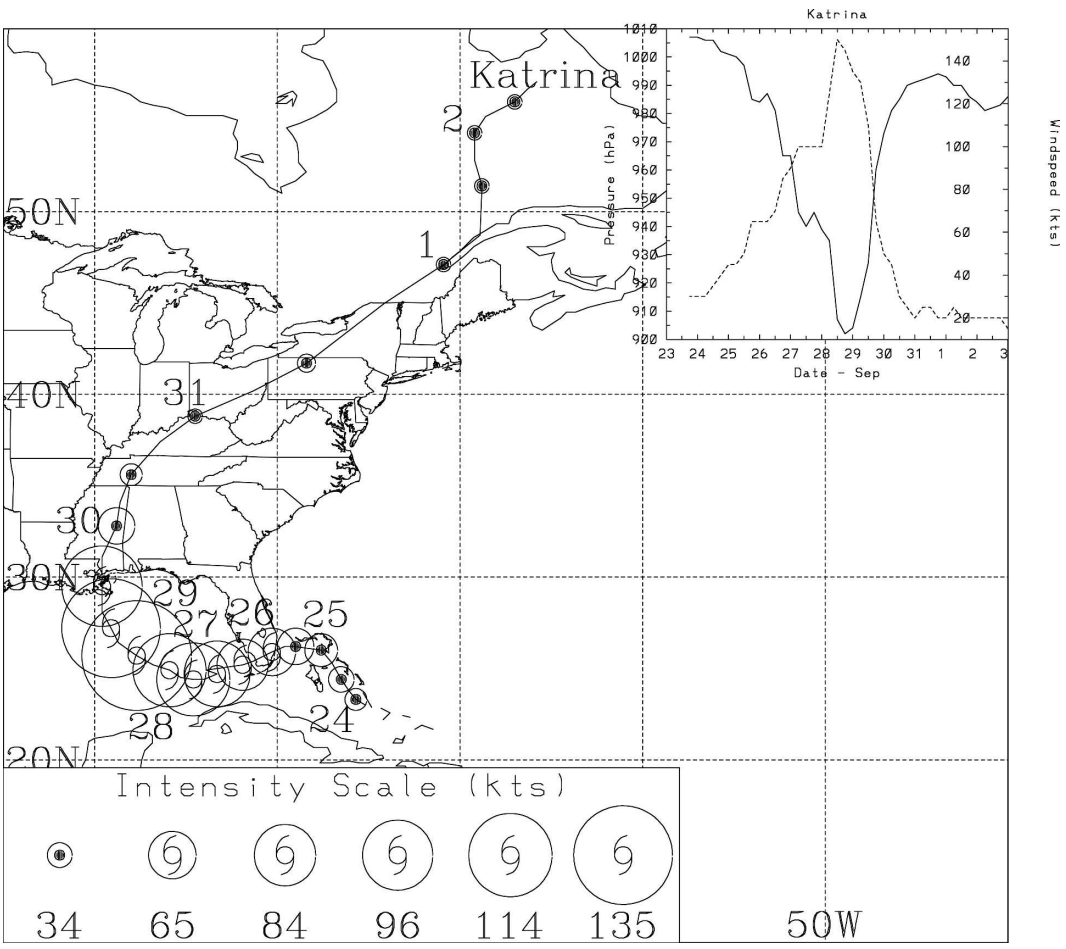

FIG. 1. Track and intensity of Hurricane Katrina as obtained from NHC advisories. The inset in the upper-right corner shows the estimated minimum sea level pressure (solid) and maximum sustained wind speed (dashed) around the storm at 6-hourly intervals.

and a minimum mean sea level pressure (MSLP) of 983 hPa. Katrina showed few signs of weakening during its brief passage over the Florida peninsula and began to intensify shortly after moving into the Gulf of Mexico early on 26 August. Two periods of rapid intensification on 26 and 28 August brought Katrina to category-5 strength with estimated near-surface winds of 77 m s^{-1} and a minimum MSLP of 902 hPa (Fig. 1). Accelerating northward, Hurricane Katrina weakened to category-3 intensity (winds near 55 m s^{-1} and a central pressure of 923 hPa) before making a pair of landfalls on the Louisiana coast. The most deadly of these was the storm's 1430 UTC 29 August landfall 35 km east of New Orleans (along the Louisiana–Mississippi border) that caused levee breaches and severe flooding in the city of New Orleans as well as widespread devastation along the Mississippi coast. Hurricane Katrina weakened rapidly after landfall, and turned to the northeast as it interacted with an upstream trough, resulting in the system's rapid extratropical transition [ET; see Jones et al. (2003) for a comprehensive review]. Despite producing heavy rain over the northeastern United States and southeastern Canada, Katrina did not reintensify following ET and eventually completed its life cycle on 7 September as it was absorbed by a preexisting extratropical low near the southern tip of Greenland.

The focus of this study is to document the complex life cycle of Hurricane Katrina, with an emphasis on interpreting the dynamic and thermodynamic structures and forcings that were active at important stages during the storm's evolution. These include the incipient vortex's development and subsequent tropical transition (TT; Davis and Bosart 2004), the storm's passage across the Florida peninsula, the pair of intensification episodes noted over the Gulf of Mexico, and the hurricane's rapid ET after landfall. The latter will emphasize the influence of the decaying system on the midlatitude flow, thereby serving as an introduction to a

companion study [McTaggart-Cowan et al. (2007), hereafter referred to as Part II] that investigates the hemispheric impacts of this strong tropical cyclone (TC).

Although earlier investigations identified the presence of upper-level troughs—generally of midlatitude origin—as a potentially important ingredient in some tropical cyclogenesis events (Sadler 1976, 1978; Bosart and Bartlo 1991; Ferreira and Schubert 1999; Bracken and Bosart 2000; Hanley et al. 2001), a conceptual model for TT was developed only recently (Davis and Bosart 2004). This model comprises two separate pathways to TT based on differing strengths of the incipient lower-level vortex. During a strong extratropical cyclone (SEC) TT, a lower-level vortex with wind speeds sufficient to trigger wind-induced surface heat exchange (WISHE; Emanuel 1987) interacts with an upstream trough or positive potential vorticity (PV) anomaly. As convection redistributes mass and momentum in the vertical, the shear related to the trough locally drops below the 10 m s^{-1} tropical genesis threshold (Zehr 1992) near the center of convection. The synoptic-scale ascent forcing leads to an increase in deep convection and the formation of a warm core system.

The weak extratropical cyclone (WEC) pathway to TT can be taken by an incipient cyclone with near-surface winds less than the 10 m s^{-1} required for initiation of the WISHE process. The trough-induced ascent and shear can initially assist in organizing convection in the local environment of the precursor vortex. The individual hot towers (Montgomery et al. 2006b) and associated vorticity may then coalesce to intensify the lower- and midlevel circulation. Once the vortex reaches an intensity sufficient to trigger WISHE, the TT proceeds as described above for the SEC case.

Once formed, continued forcing from the local environment can have a strong influence on the strength and nature of TCs, particularly if the change occurs at the lower boundary. The processes involved with the spindown of hurricanes after landfall have been understood for some time (e.g., Hubert 1955; Miller 1964; and many others) to be a combination of frictional drag, reduced sensible and latent heat fluxes, and interaction with orography. The role played by sea surface temperature (SST) in determining the strength of TCs has been less well defined despite the existence of the 26.5°C SST threshold (Gray 1968). Shay et al. (2000) show that a warm core ring (WCR) combined with jet and trough dynamics (Bosart et al. 2000) to induce the rapid intensification of Hurricane Opal (1995) over the Gulf of Mexico. The authors hypothesize that the depth of warm water in the WCR reduces the mixing-driven cooling induced by the hurricane, a process that can cool SSTs beneath the storm by 6°C or more (e.g., Bender et al. 1993; among others).

The effects of a perturbed synoptic-scale environment on a TC can be even more dramatic than those related to changes to surface properties. At its most intense, tropical–midlatitude interaction can lead to the ET of the storm, an event that signals the end of the tropical phase of the system's life cycle. The process of ET has recently received significant attention in the literature [Jones et al. (2003) present a summary of current ET research] in the form of climatological studies (Hart and Evans 2001), case studies (Atallah and Bosart 2003; Abraham et al. 2004; Atallah et al. 2007), and modeling studies (McTaggart-Cowan et al. 2003; Colle 2003)]. Recent work by Anwender et al. (2006) and Harr et al. (2006) has shown that ET events—in particular those that lead to redevelopment—present a significant challenge to both deterministic and ensemble forecasting systems. Harr et al. (2006) demonstrate that uncertainty associated with transitioning systems in the western North Pacific Ocean can readily impact medium-range forecasts over North America through the excitation of Rossby waves. As will be shown in Part II, these perturbations to the midlatitude flow can persist for several weeks even following a decaying ET event, and can result in further interaction between the Tropics and the extratropics.

This study begins with a description of the data and methods used to document the complex life cycle of Hurricane Katrina in section 2. Section 3 investigates Katrina's genesis following the WEC pathway. The subsequent track and evolution of the storm, including the effects of its interaction with the Florida peninsula and final landfall in Louisiana, are investigated in section 4. The ET stage of Katrina's life cycle is documented in section 5. The study concludes with section 6, which is a brief summary and discussion of the findings.

2. Data and methods

Basic information for Hurricane Katrina and the storms in the Florida landfall climatology (section 4b) has been derived from the NHC best-track archive (track and intensity) and NHC advisories (storm radius). Global 0.5° gridded analysis data from the National Centers for Environmental Prediction Global Forecast System are used throughout this study for the computation of atmospheric diagnostics. Analyses of SST have been performed using the National Oceanic and Atmospheric Administration (NOAA) optimum interpolation SST (version 2) dataset with 1° grid spacing (available online at http://www.cdc.noaa.gov/cdc/

TABLE 1. Reference table for symbols used in the text and figures.

Symbol	Description	Sections	Figs.
A	Gulf Coast anticyclone	4a, 4c	8
B	Bermuda anticyclone	4a	8
C	Cold upper-level air	3a	4
G	Low-latitude trough	3a, 4a	4, 8
K	Hurricane Katrina	3a, 3b, 5	4, 6, 8, 15
O	Outflow from Katrina	4c, 5	8, 15
R	Remnant TD-10 vortex	3b	6
U	Upstream trough	4c, 5	8
V	Easterly wave	3b	6

data.noaa.oisst.v2.html). A summary of the annotations used throughout the text is provided in Table 1.

This investigation also makes extensive use of satellite brightness temperatures from the Geostationary Operational Environmental Satellites (GOES) infrared channels obtained from the Unidata Local Data Manager (available online at http://www.unidata.ucar.edu/software/ldm) with an approximate 0.2° grid spacing. The brightness temperatures recorded by the GOES are closely related to the temperature of the highest cloud layer, or to the surface temperature in cloud-free areas. Data from the satellites *Jason-1*, the Ocean Topography Experiment (TOPEX)/Poseidon, *Environmental Satellite* (*Envisat*), and *Geosat Follow-On* were combined to create the altimetry dataset used in the analysis of Katrina's rapid intensification in section 4c (Scharroo et al. 2005).

The Rossby penetration depth ($\mathcal{R}$) referred to in section 3a is computed as

$$\mathcal{R} = L\left(\frac{f_0^2}{N^2}\right)^{1/2}, \tag{1}$$

where N^2 is the square of the Brunt–Väisälä frequency, f_0 is the reference Coriolis parameter (5×10^{-5} s^{-1} in this study, representing the planetary value near 20°N), and L is the characteristic horizontal length scale of the system (here taken to be 1000 km). The influence of a PV anomaly decays with a vertical scale of $(\frac{1}{2})\mathcal{R}$ (Hoskins et al. 1985; Zurita and Lindzen 2001).

The power dissipation (PD) described in section 4d is based on the formula presented by Emanuel (2005) in axisymmetric instantaneous form:

$$\mathrm{PD}(t) = 2\pi \int_0^{r_0} C_D \rho V(r)^3 r\, dr, \tag{2}$$

where r is the radius from the center of the hurricane, C_D is the drag coefficient, ρ is the air density, V is the near-surface wind speed as a function of r only, and r_0 is the outer storm radius. Because the three-dimensional structure of the near-surface wind field is poorly represented in coarse analysis data, we employ a standard Rankine vortex model in which

$$V(r) = \begin{Bmatrix} V_{\max}\left(\dfrac{r}{R}\right) & \text{for} \quad r < R \\ \dfrac{RV_{\max}}{r} & \text{for} \quad r > R \end{Bmatrix}, \tag{3}$$

where R is the radius of maximum winds ($V_{\max}$). Substituting (3) into (2) allows for the development of an analytic solution of the following form:

$$\mathrm{PD}(t) = 2\pi R^2 C_D \rho V_{\max}^3 \left(\frac{6}{5} - \frac{R}{r_0}\right), \tag{4}$$

which is based only on the readily observable parameters $V_{\max}$ (best-track intensity data), R (eyewall radius from satellite imagery and airborne Doppler radar data provided by the NOAA Hurricane Research Division of the Atlantic Oceanographic and Meteorological Laboratory), and r_0 [tropical storm (TS)-force wind radius from NHC advisories]. The density is set constant at 1.2 kg m^{-3} and C_D varies weakly with $V_{\max}$ as described by Powell et al. (2003).

3. Tropical transition

Hurricane Katrina was first identified by the NHC as TD 12 at 1800 UTC 23 August 300 km southeast of Nassau, Bahamas. The storm's initiation followed the WEC pathway described by Davis and Bosart (2004), in which a preexisting lower- to midlevel vortex interacts with a low-latitude upper-level trough to initiate TT. Each of these features will be described in detail in this section using Fig. 2 as a reference. The figure displays the mean conditions over the western Atlantic and the Caribbean Sea for the 1-week period leading up to Katrina's development. The midlatitude trough (section 3a) is recognizable as an area of increased pressure on the dynamic tropopause [p_{DT}, where the dynamic tropopause is defined as the 2-PVU surface (1 PVU $\equiv$ 10^{-6} m^2 K kg^{-1} s^{-1})], while the lower-level vortex (shown at 0000 UTC 17 August in the Fig. 2 inset, and discussed in section 3b) is tracked as it passes through a region of persistent convection and into the Caribbean Sea.

a. Midlatitude trough

The presence of a midlatitude trough or PV tail is crucial to the TT model of Davis and Bosart (2004). During Katrina's initial development, the trough (Fig. 2) provides three separate forcings that assist with the genesis process. First, it provides a broad region of deep background cyclonic vorticity at low latitudes where the

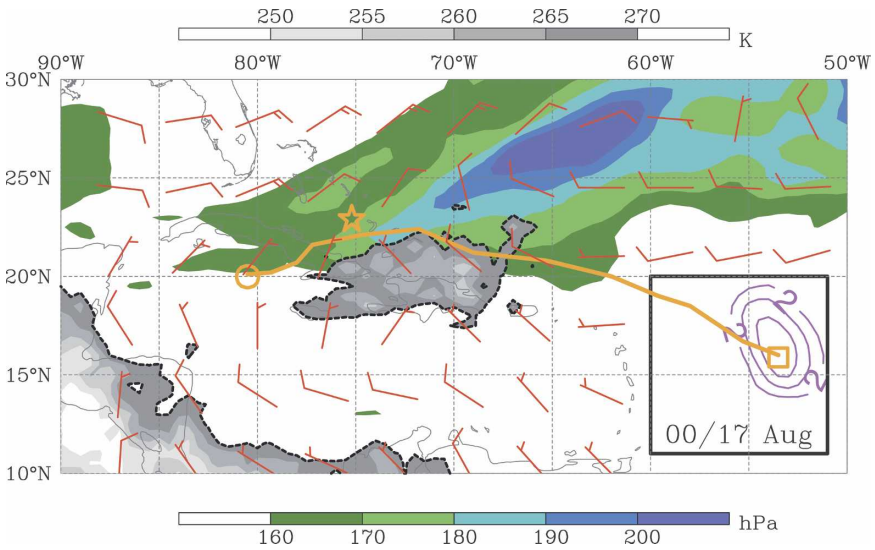

FIG. 2. Mean conditions over the western equatorial Atlantic Ocean from 0000 UTC 17 Aug to 1800 UTC 23 Aug 2005. Winds on the DT are plotted in red with long and short barbs corresponding to 5 and 2.5 m s^{-1} wind speeds, respectively. Pressure on the DT is shown in color at 10-hPa intervals as indicated on the color bar. Gray shading represents mean satellite brightness temperatures scaled according to the grayscale bar at the top of the plot with a dashed contour indicating 270 K. The inset shows the TD-10 remnant at 0000 UTC 17 Aug 2005 using the 850-hPa relative vorticity at 2×10^{-5} s^{-1} intervals with magenta contours. The track of the TD-10 vortex is shown in orange from 0000 UTC 17 Aug (square) to 0000 UTC 23 Aug 2005 (circle), as is Katrina's initial location at 0000 UTC 23 Aug 2005 (star).

Coriolis force is small. This relative vorticity can be effectively stretched by convectively driven ascent. Second, the p_{DT} maximum implies the presence of a mid- to upper-tropospheric cold pool beneath the trough that simultaneously reduces the local bulk column stability. Third, advection of high p_{DT} air over a relatively quiescent lower-level flow results in the formation of a quasigeostrophically forced ascent region downshear of the trough axis by differential vorticity advection. The phasing of this cyclogenetically favored region with a lower-level positive PV disturbance of either baroclinic or convective origin can lead to the mutual intensification of the systems (Eady 1949; Hoskins et al. 1985).

The aforementioned trough was a persistent feature over Cuba and the Bahamas for the week leading up to Katrina's initiation as shown in Fig. 2. Its importance is highlighted by an area of persistent enhanced convection (indicated by cold brightness temperatures recorded from the cloud tops) over eastern Cuba and Hispaniola between 17 and 23 August. Katrina's NHC-defined genesis point (indicated by the star in Fig. 2) is 300 km north of this synoptically forced convective region, but the analysis to be presented in section 3b shows that the incipient vortex is triggered within this area of long-lived convection.

The structure of the midlatitude trough at 1200 UTC 23 August is shown in Figs. 3 and 4. An east–west trough in the upper-level thickness field (heavy solid line in Fig. 3a) combines with potentially cold upper-level (150–200 hPa) air over eastern Cuba (labeled "C" in Fig. 4) to produce a broad region of enhanced potential intensity (PI; Bister and Emanuel 1997), into which Katrina moves shortly after its development on the eastern periphery of the local PI maximum. Also associated with this area of cool air aloft is a maximum in $\mathcal{R}$ (Fig. 3b). This allows the upper-level positive PV in the region to extend its influence over a deeper layer of the atmosphere, further enhancing the effects of convectively induced stretching on vorticity generation. A cross section taken along the northeasterly upper-level flow (Fig. 4) demonstrates the presence of both potentially cool air beneath the trough (labeled "G" in Fig. 4) and strong differential vorticity advection downshear of the local vorticity maximum. This quasigeostrophic ascent forcing is collocated with the incipient lower-level vortex (labeled "K") also evident in Fig. 4.

b. *Lower-level vortex*

Despite the persistent nature of the trough and its cyclogenetic forcing, a lower-level vortex is required to trigger development under the WEC paradigm. This feature may be, for example, a remnant extratropical

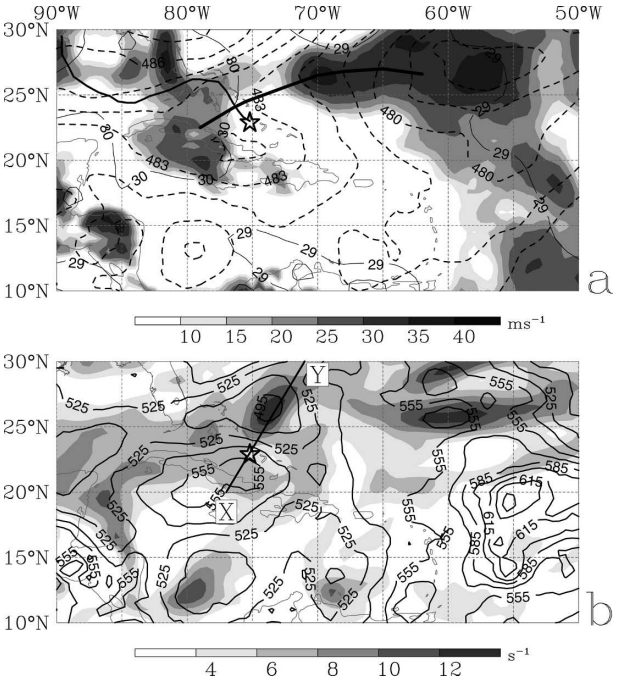

FIG. 3. Conditions at 1200 UTC 23 Aug 2005, 6 h before the first NHC advisory for TD 12 (Katrina). (a) Upper-level thickness (200–400 hPa, dashed contours at 1-dam intervals) and surface PI (shaded, with values as indicated on the grayscale bar). (b) Upper-level relative vorticity (mean 200–400 hPa, shading as indicated on the grayscale bar) and $\mathcal{R}$ (in the 200–400-hPa layer, solid contours at 15-dam intervals). Katrina's initial location is shown with a star in both plots, and the storm's track is indicated with a thin solid line in (a). The heavy solid line in (a) highlights the upper-level thermal trough and the solid line in (b) shows the cross-sectional axis for Fig. 4 with symbols X and Y providing references for orientation.

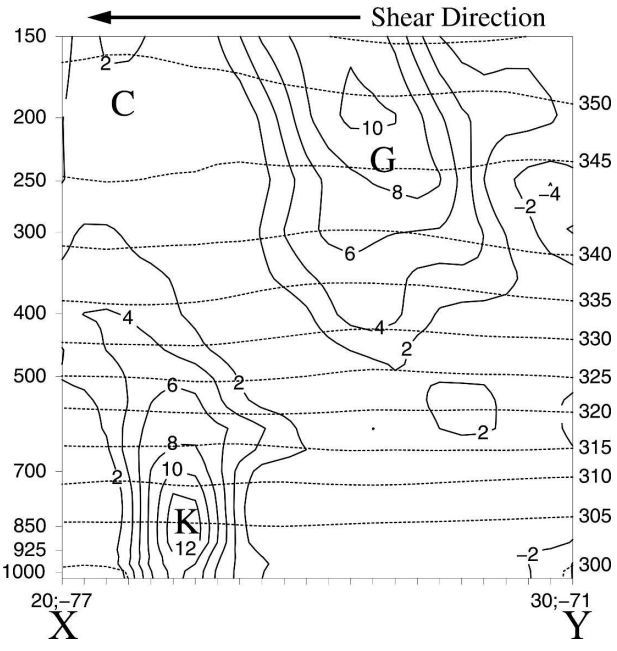

FIG. 4. Cross section of along the line X–Y shown in Fig. 3b. Relative vorticity is shown in solid contours at intervals of 2×10^{-5} s^{-1} overlaid with potential temperature (dashed contours at intervals of 5 K). Annotations follow the text and are summarized in Table 1.

circulation (Powers and Davis 2002), a mesoscale convective vortex (Bosart and Sanders 1981; Simpson et al. 1997; Molinari et al. 2004), or the remains of a previous tropical cyclone (as in this case).

The primary lower- to midlevel vortex that assists with the development of Hurricane Katrina is the remnant circulation of TD 10, which formed in the central Atlantic Ocean from an easterly wave precursor at 2100 UTC 13 August. Infrared satellite imagery for 10–24 August (Fig. 5) shows the progression of a well-defined easterly wave from 30°W (Fig. 5a) to the location of TD 10 as indicated by the white box in Figs. 5i,j. Although TD 10 dissipates after only 18 h (at 1500 UTC 14 August) because of strong environmental shear, the region of cloudiness associated with its remnant vortex can be readily tracked at a relatively constant phase speed westward until 20 August (Fig. 5u). After this time, the TD-10 vortex becomes difficult to distinguish from the broad area of convection in the eastern Caribbean forced by the trough (section 3a).

The remnant circulation of TD 10 plays an important role in the organization of convection north of Hispaniola as it moves through the Bahamas on 20 and 21 August; however, it maintains its identity in the lower-level relative vorticity fields shown in Fig. 6 (labeled as remnant "R") and continues to track westward over Cuba (Fig. 2). Following the passage of the TD-10 vortex (R), the vorticity maximum associated with the long-lived convection downshear of the trough (Fig. 2) grows in both size and strength (Fig. 6d). A second, weaker and initially dry easterly wave follows the TD-10 remnant through the region on 22 August and continues westward according to the 0000 23 August analysis (labeled easterly wave "V" in Figs. 6b–h and tracked at 6-hourly intervals during the analysis to ensure continuity). Immediately after this second round of convective organization, the persistent vorticity maximum over Hispaniola extends northwestward toward a region of enhanced PI (Fig. 3a) and begins to intensify as its structure develops (labeled "K" in Fig. 6h). It is this feature that tracks into the Bahamas on 23 August to become the nascent Katrina by 0000 UTC 24 August (solid circle outline in Fig. 5cc).

4. Track and intensity

Hurricane Katrina's structure and intensity both undergo periods of rapid evolution during the tropical

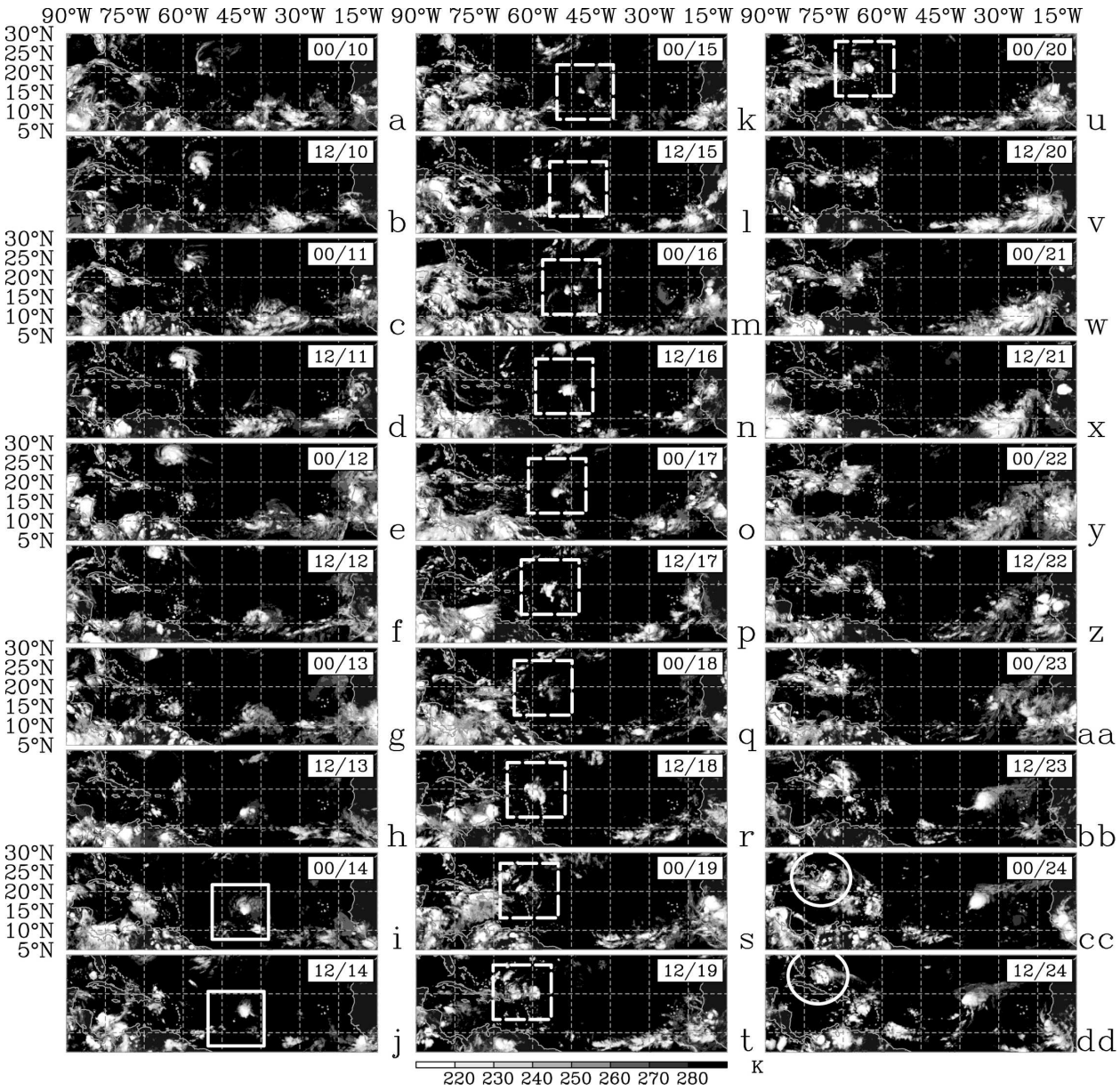

FIG. 5. Infrared GOES satellite mosaic at 12-h intervals from (a) 0030 UTC 10 Aug to (dd) 1230 UTC 24 Aug 2005. (i), (j) The advisory location of TD 10 is shown by the white squares, (k)–(u) dashed white squares track the remnant TD-10 vortex, and (cc), (dd) the best-track location of TD 12 (Katrina) is indicated by the solid white circles. Times–dates are shown as two digit hour–day sets.

phase of the storm's life cycle. Figure 7 shows these quantities at selected times along the hurricane's track. The physical mechanisms behind Katrina's movement, rapid axisymmetrization, and pulsed intensification summarized in Fig. 7 will be assessed in detail in this section.

a. Initial intensification

Following Katrina's genesis as TD 12 on 23 August, the developing vortex drifts slowly northwestward along the eastern Bahamas, steered by a ridge over the central equatorial Atlantic (labeled "B" in Fig. 8) that folds over the trough associated with storm's initiation (described in section 3a and labeled "G" in Fig. 8). This track takes the developing storm over anomalously warm waters (>1.0°C above climatology) southeast of the Florida peninsula, with SST values over 30°C (Fig. 9a). As shown in Fig. 10, the deep layer vertical shear over the system remains below 10 m s^{-1} (a critical value for development as defined by DeMaria 1996) follow-

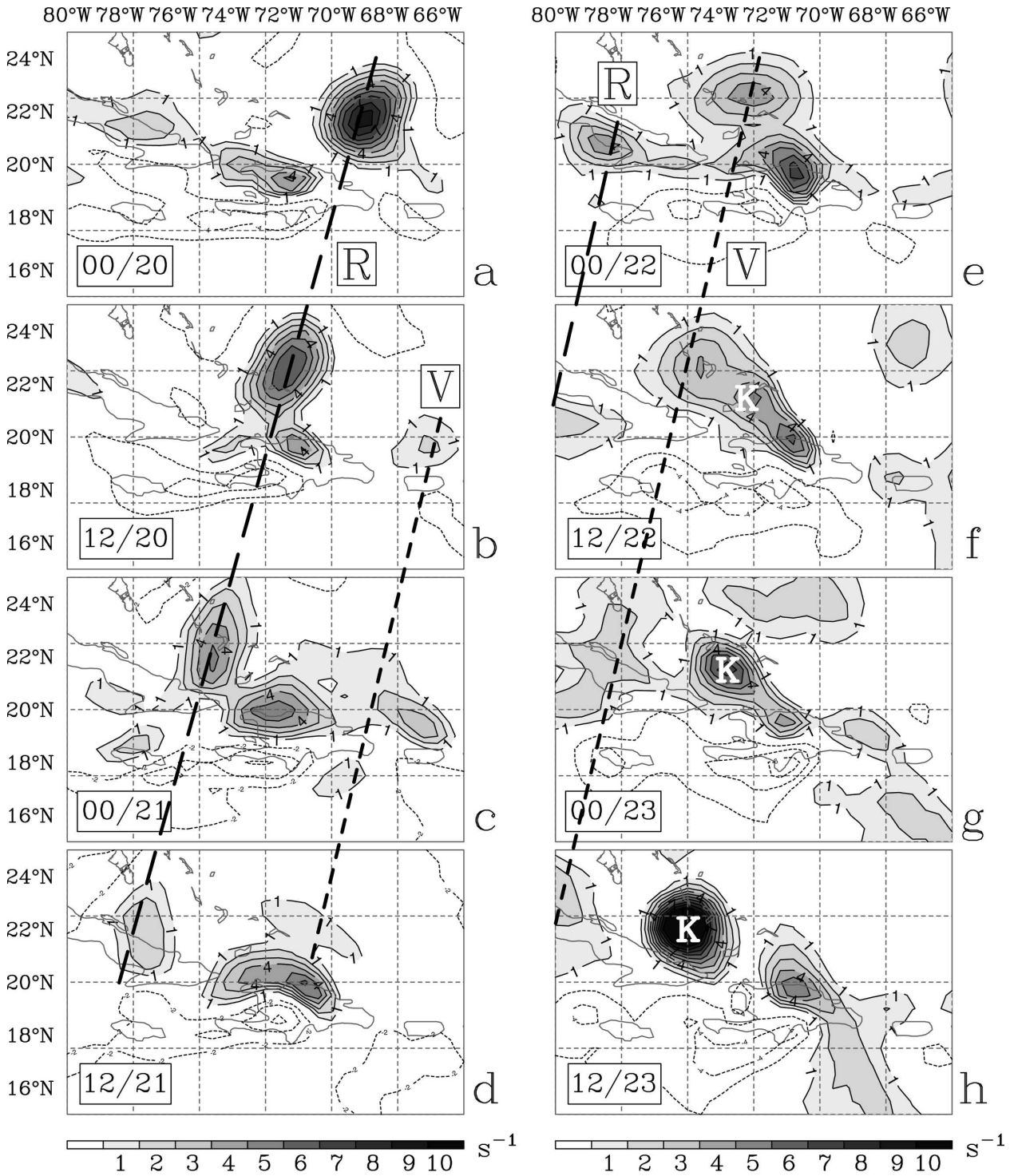

FIG. 6. Mean 925–850-hPa relative vorticity, positive values shaded and contoured at 1×10^{-5} s^{-1} intervals as indicated on the grayscale bar, negative values shown with dashed contours plotted at 2×10^{-5} s^{-1} intervals. Times–dates are plotted the same as in Fig. 5. The progression of the TD-10 remnant [(a), (e) labeled "R"] is emphasized by the (a)–(f) heavy long-dashed line and the easterly wave precursor [(b), (e) labeled "V"] is tracked with the (b)–(h) heavy short-dashed line. (f)–(h) Katrina's incipient vortex at 1200 UTC 23 Aug 2005 is labeled "K."

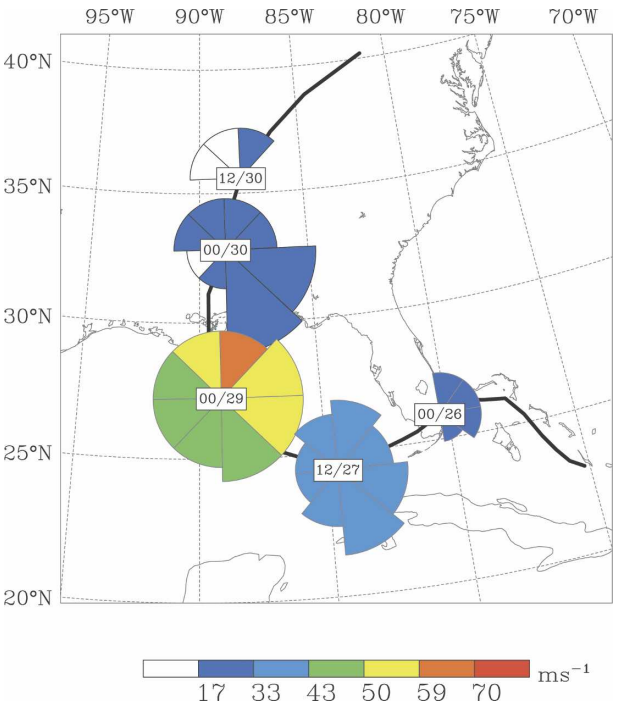

FIG. 7. Summary plot of Hurricane Katrina's life cycle. The storm's track is shown indicated with the heavy black line, with near-surface winds (30-m level) from the 0.5° GFS analysis used to determine intensity and structure at selected times as indicated (times–dates plotted the same as in Fig. 5). The radius of each slice indicates the geographic extent of either TS-force winds (17.5 m s^{-1}, slices outlined in magenta) or 10 m s^{-1} winds (slices outlined in black). The maximum wind speed observed in each slice is used to choose an intensity level for that eighth of the storm, with magnitudes as indicated on the color bar.

ing the TT of the incipient vortex and its associated destruction of the PV tail to the west of trough G through diabatic vertical redistribution of PV (Figs. 8a–c). The combined effects of the warm underlying sea surface and weak vertical shear allow Katrina to intensify as it moves through the Bahamas. By 0000 UTC 25 August, the fold-over ridge responsible for the storm's northward trajectory (B in Fig. 8c) had moved into the central Atlantic and a region of elevated θ_{DT} over the western U.S. Gulf Coast (labeled "A" in Fig. 8) becomes the primary steering influence for Katrina. Accordingly, the storm makes a cyclonic track change and takes up a westerly heading toward the southern Florida peninsula. As the distance between the like-signed θ_{DT} anomalies A and B (Figs. 8a–d) increases, the destructive interaction between them weakens and the northeasterly shear over Katrina slowly begins to rise (Fig. 10). Despite this increase, shear values remain below the critical level for the organizing vortex, and warm SSTs along the eastern Florida coast (Fig. 9a) lead to high PI values in the system's environment (Fig. 10). Despite asymmetries in the cloud field (Figs. 11b,c), Katrina reaches category-1 hurricane status shortly before 0000 UTC 26 August, just prior to its first landfall near Miami.

b. *The Florida peninsula: Katrina and climatology*

With winds gusting over 38 m s^{-1}, Katrina's landfall on the southern Florida peninsula results in significant damage and the loss of 14 lives (Knabb et al. 2005). The evolution of the storm's structure during its passage across the low-lying landmass is well documented by the NOAA Weather Surveillance Radar-1988 Doppler (WSR-88D) radar based in Miami (KAMX; Fig. 12). As shown in Figs. 11b,c, Katrina remains a relatively poorly organized system east of Florida with only isolated cloud tops at temperatures below 220 K. This evaluation of Katrina's structure is consistent with the lack of a complete encircling eyewall at 1800 UTC 25 August (Fig. 12a). Although there is extensive deep convection near the core, there is suppressed convective activity particularly in the northwestern quadrant of the eyewall. As landfall occurs, however, the missing eyewall segments fill in, and a well-defined eye takes shape (Fig. 12c). A broad inflow region over the warm coastal waters to the west of the Florida peninsula (Figs. 9a and 12c) fuels enhanced convection to the south of the system that wraps inward toward the core as Katrina begins to move over land (Figs. 11c and 12d). Despite a reduction in the extent of reflectivity maxima north of the center (Fig. 12e), the convective activity in the southern quadrant of the storm appears to be sufficient to maintain the system as it completes its 6-h passage across the peninsula (Fig. 12f). By 0800 UTC the center of circulation had moved into the Gulf of Mexico, accompanied by a strengthening convective outbreak over the Florida Keys. Temporarily downgraded to tropical storm (TS) status at 0600 UTC 26 August after wind estimates drop from 35 to 30 m s^{-1}, Katrina quickly redevelops as a hurricane and begins its first period of rapid intensification (Fig. 10). The structure of the storm by 27 August is notably larger and more symmetric than it was before Katrina's landfall in southern Florida (Figs. 7 and 11d).

The landfall stage of a hurricane's life cycle is usually characterized by rapid weakening as increased surface drag and decreased sensible and latent heat fluxes act in combination to induce the spindown of the vortex (e.g., Bergeron 1954; Hubert 1955; Miller 1964, and many others since then). In Katrina's case, however, the circulation left the Florida peninsula only 5 m s^{-1} weaker, and with a better-defined eye than it had leading up to its interaction with the landmass. To determine

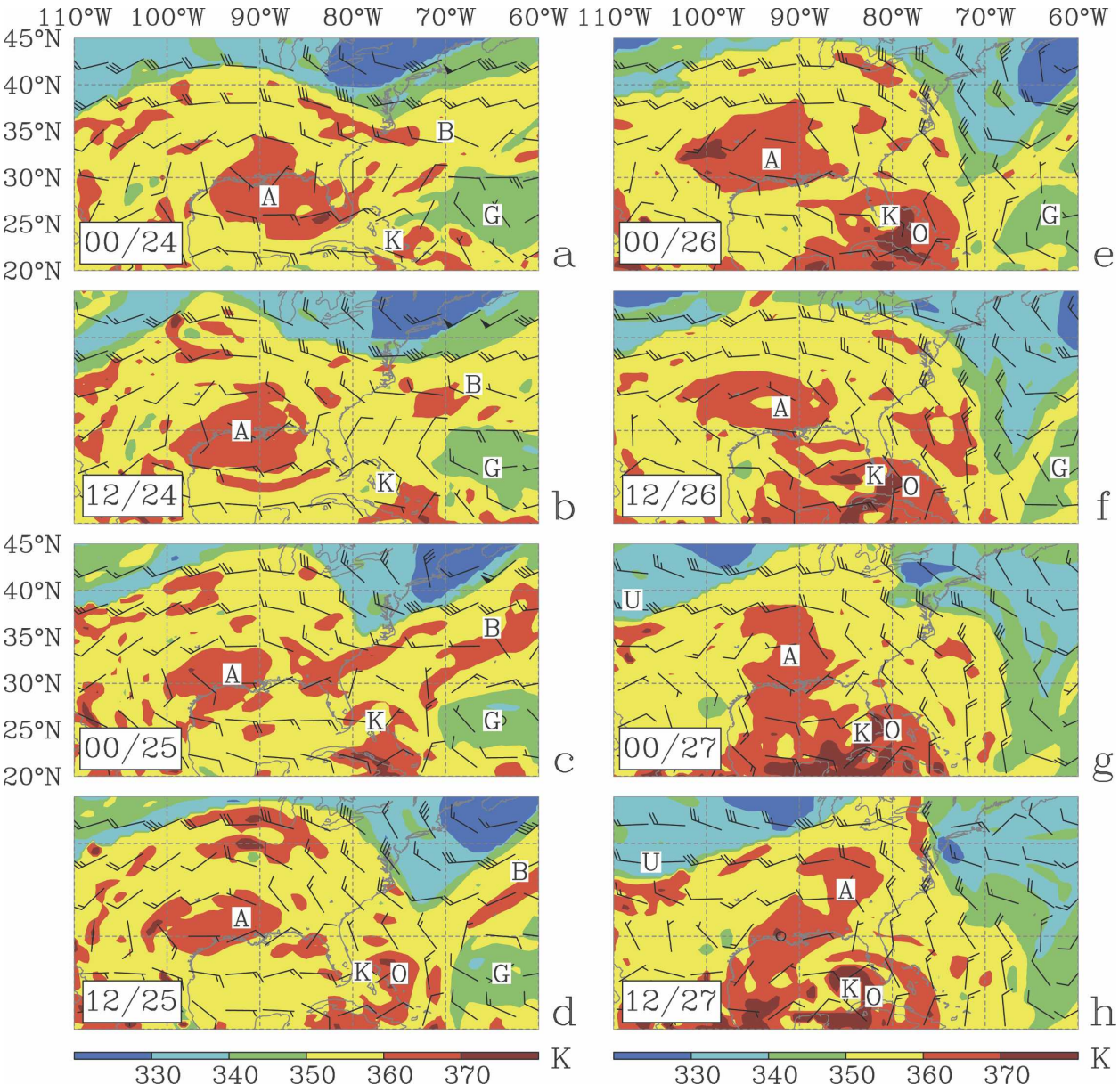

FIG. 8. Dynamic tropopause potential temperature (θ_{DT}) at 12-hourly intervals from (a) 0000 UTC 24 Aug to (p) 1200 UTC 31 Aug 2005 at 10-K intervals as indicated on the color bar. Winds on the DT are plotted with pennants, long and short barbs corresponding to 10, 5, and 2.5 m s^{-1} wind speeds, respectively. Annotations follow the text and are summarized in Table 1. Times–dates are plotted the same as in Fig. 5.

whether Katrina's demonstrated insensitivity to the presence of the Florida peninsula is an unusual occurrence, or whether storms crossing the Everglades-dominated region do not typically weaken significantly, a climatology of hurricane traverses of southern Florida is developed here. The criteria for case selection were

- named storm (implies 1954–the present);
- passes through a 2° latitude–longitude box centered on (26°N, 81°W); and
- crosses south Florida on a zonal track or remains over land for less than 12 h.

Using the these criteria, eight cases were identified in the NHC best-track archive (Table 2 and Fig. 13). Hurricane Katrina was not included in the dataset to avoid possible contamination of the results. A "two one-sided test" ("TOST") equivalence testing strategy (Schuirmann 1987) was used to determine whether a significant weakening trend was detectable in the climatology

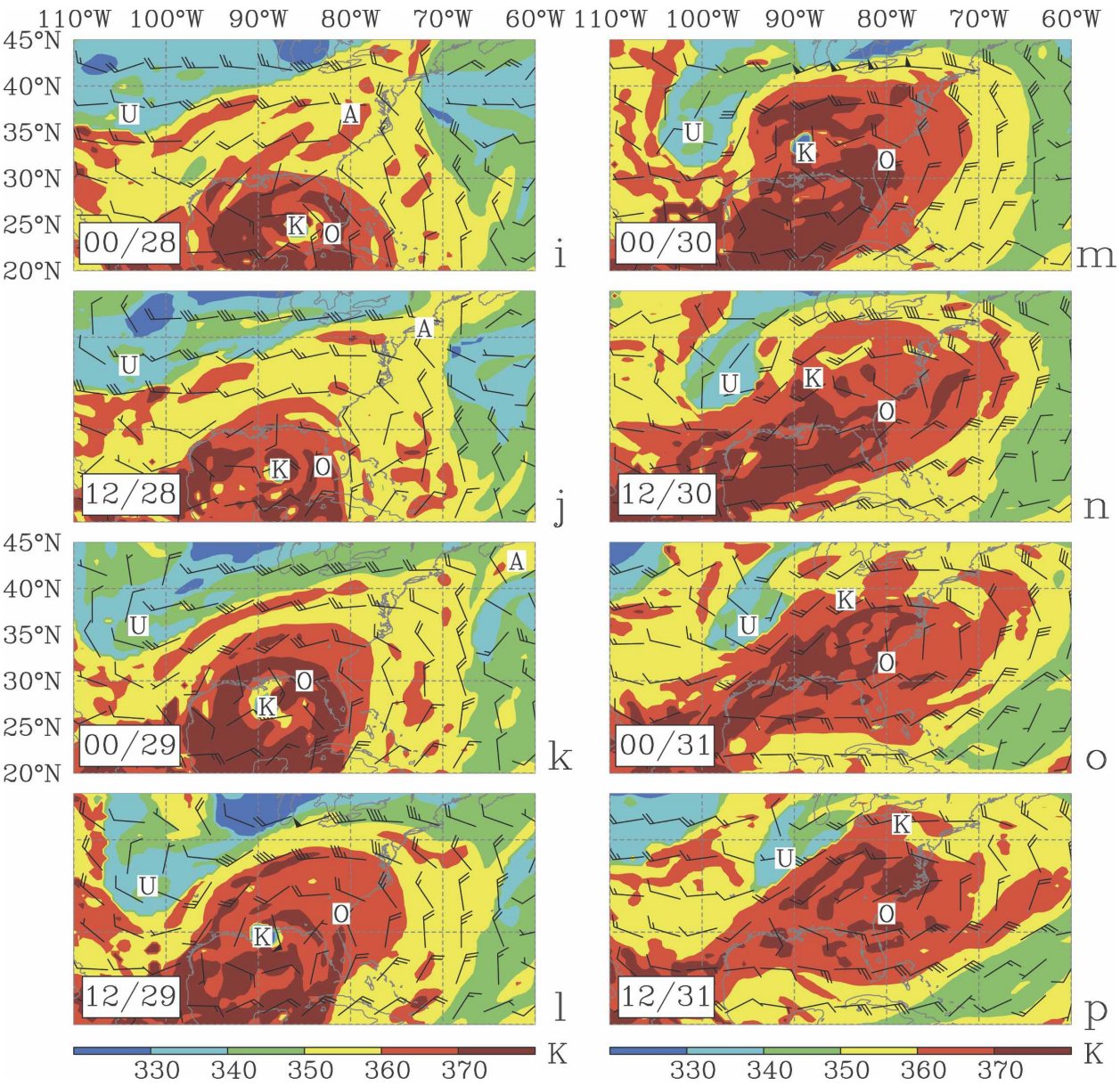

FIG. 8. (*Continued*)

of southern Florida landfalls. The landfalling sample data were defined as the change in best-track wind speeds between the analysis time 6–12 h before landfall and 6–12 h after leaving the peninsula. In practice, the residence times of the selected storms over the Florida peninsula were short (because of the final criterion above and the width of the peninsula) and the time difference was 24 h in each case. The population was therefore drawn from the 24-hourly differences in storm intensity during the remainder of the systems' life cycles, both leading up to and following their landfalls in Florida. To avoid biasing the results toward rejection of the null hypothesis, prior and subsequent landfalls were also masked from the dataset. To ensure the independence of the population samples, the intensity change was computed at 2-day intervals so that intensity trends lasting for up to 48 h would not exert an unjustifiably large influence on the results.

The null and alternative hypotheses for the equivalence test, H_0 and H_1, respectively, amount to an interval hypothesis for the equivalence interval $[V_1, V_2]$ of the following form:

$$H_0: \mu_s - \mu_p \leq V_1 \quad \text{or} \quad \mu_s - \mu_p \geq V_2, \tag{5}$$

$$H_1: V_1 < \mu_s - \mu_p < V_2. \tag{6}$$

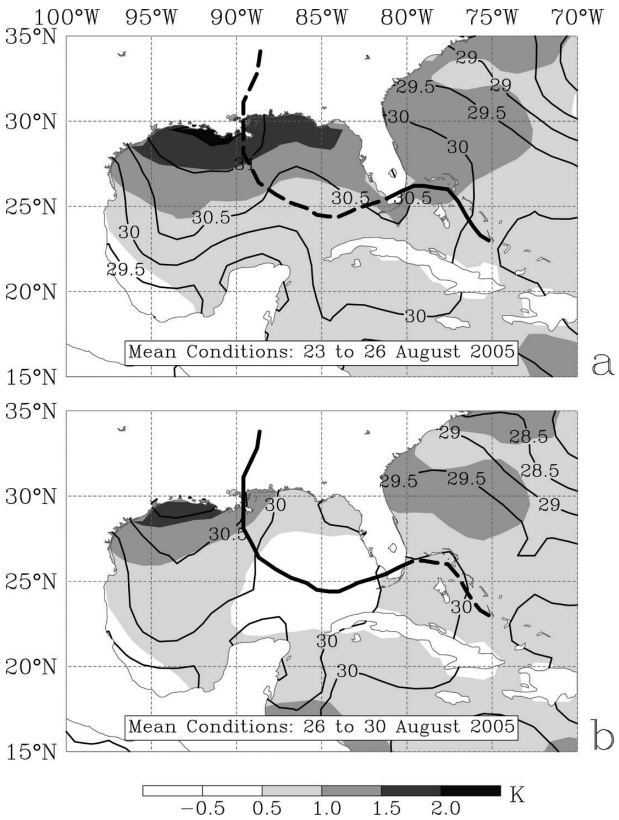

FIG. 9. Mean SST (solid black contours at 0.5-K intervals) and anomalous SST (shaded with values as indicated on the grayscale bar) for (a) 23–26 and (b) 26–30 Aug 2005. The track of Katrina over the averaging period is shown with a heavy solid line. Katrina's track at times outside the period are shown with heavy dashes.

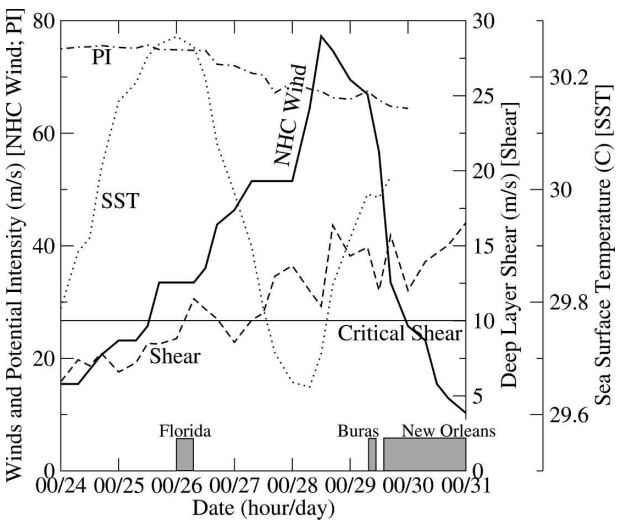

FIG. 10. Storm centered time series of near-storm values averaged over a 5° by 5° box centered on Katrina's best-track location (best-track winds, PI, DT-850 hPa shear, and SST). Land is masked for SST and PI averaging. Landfall periods are indicated along the abscissa by shaded boxes.

Here, subscripts s and p refer to the sample (landfalling) and population (tropical life cycle) datasets, respectively; μ is the mean of each set; and V_1 and V_2 are chosen symmetrically as -10 and 10 m s^{-1} to represent variations on the order of a single Simpson (1974) hurricane category (this is also below the 13 m s^{-1} standard deviation of the population as shown in Table 3). Rejection of the null hypothesis would imply that there is no significant difference between the evolution of hurricanes' intensity over the Florida peninsula and natural variability over the remainder of the tropical phase of the storms' life cycles. In essence, this would suggest that southern Florida does not exert significant weakening (or strengthening) forcings on TCs in the climatology.

As shown in Table 4, application of the TOST equivalence test reveals that the null hypothesis is rejected at the 95% level, demonstrating that landfall on the southern Florida peninsula does not lead to the initiation of a statistically significant intensity trend. Katrina is therefore not unusual in its insensitivity to the presence of the Florida landmass.

The minimal zonal extent of Florida means that much of the storm's inflow spends the majority of its time over warm Gulf of Mexico or Gulf Stream waters (Fig. 9). Additionally, the lack of orographic features in the southern peninsula region ensures that no terrain-induced flows disrupt the circulation of a landfalling hurricane. This factor is evidenced by the superior structure of Katrina as it entered the Gulf of Mexico (Figs. 12f and 11d). Finally, the abundantly available moisture in the swamplike Everglades ensures that latent heat fluxes generally remain positive (toward the atmosphere). This allows the necessary convective destabilization of the lower layers to continue despite the storm's passage over land. From a forecasting perspective, provided that the conditions for this analog study (listed above) are met, these factors in general combine to allow TCs to cross the Florida peninsula without undergoing significant weakening in intensity.

c. *Intensification and final landfall*

Hurricane Katrina's entry into the Gulf of Mexico at 0600 UTC 26 August is followed by the onset of the first of two periods of rapid intensification. Over the subsequent 24-h period, the storm's maximum estimated wind speeds increase from 33 to 51 m s^{-1}. The dominant feature in the area remains the broad anticyclone A (Fig. 8) centered over the western U.S. Gulf Coast states. This ridge continues to steer Katrina west-

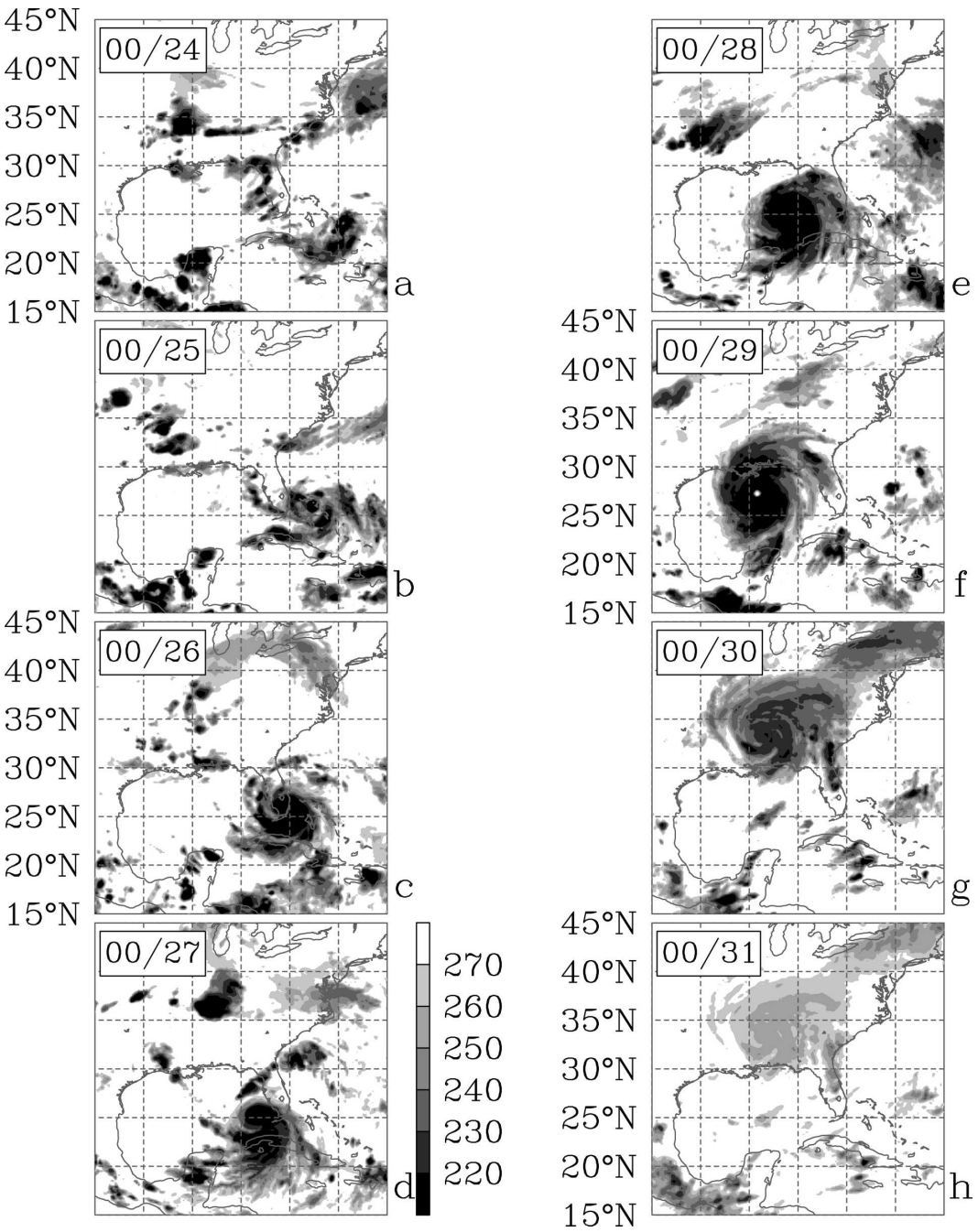

FIG. 11. Infrared GOES satellite images at 24-hourly intervals from (a) 0000 UTC 24 Aug to (h) 0000 UTC 31 Aug 2005. (d) Observed brightness temperatures (K) are plotted as indicated on the grayscale bar. Times–dates are plotted the same as in Fig. 5.

ward while shear stays constant near 10 m s^{-1} (Fig. 10). The developing convective outflow from the storm (labeled "O" in Fig. 8) negatively influences the accuracy of the vertical shear calculation and the increasingly symmetric cloud structures shown in Figs. 11c–f suggest that Katrina is effectively shielded from environmental shear between 26 and 28 August by its own strong outflow anticyclone. Although dropping slightly, the PI values in the near-storm environment remain high (above 70 m s^{-1}, Fig. 10) despite the presence of the nearby θ_{DT} maximum. The warm SSTs of the Gulf of Mexico (>29.5°C as shown in Fig. 9b) are responsible

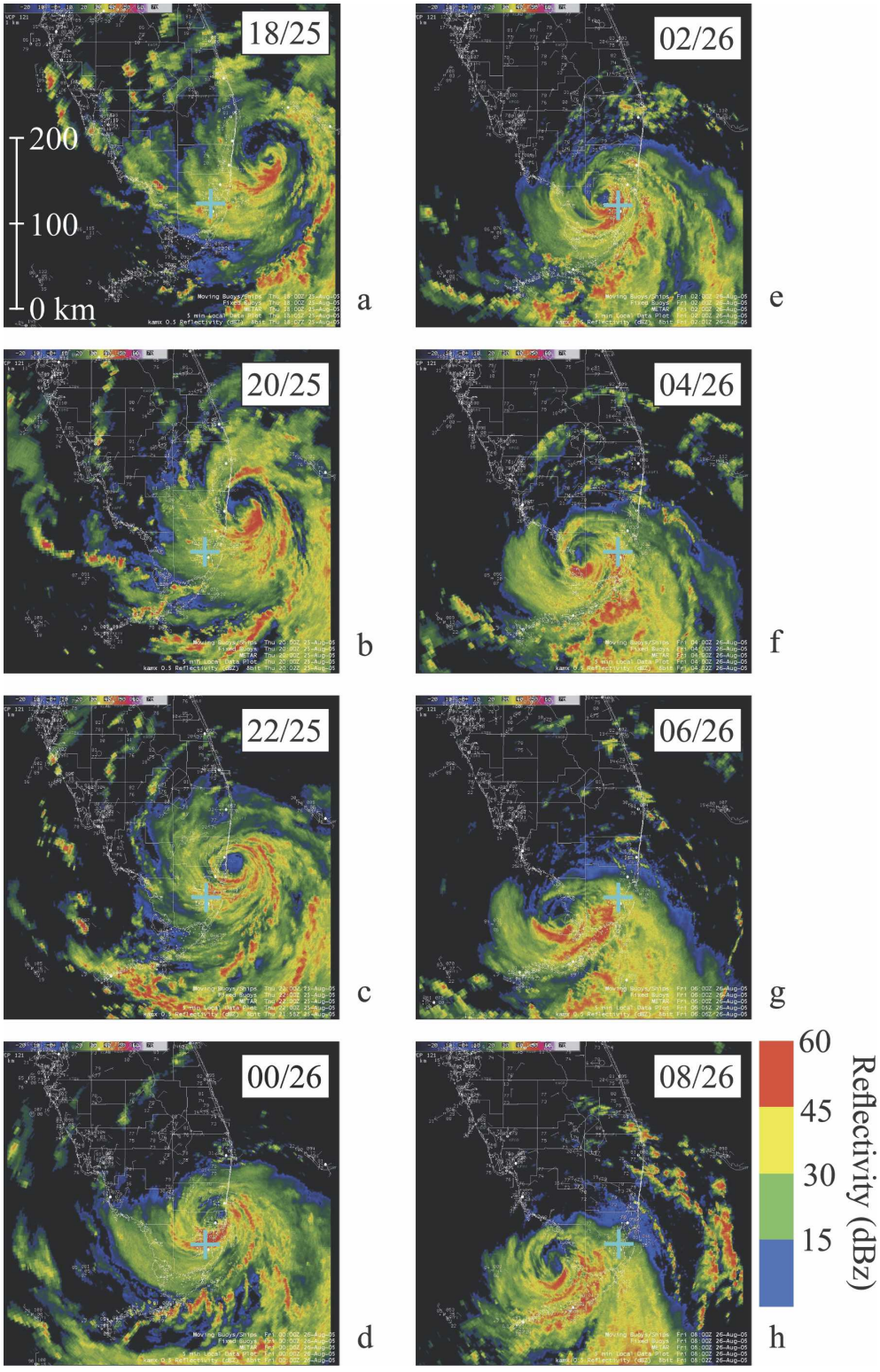

FIG. 12. Low angle (0.5°) reflectivity recorded by the Miami WSR-88D radar at 2-hourly intervals from (a) 1800 UTC 25 Aug to (h) 0800 UTC 26 Aug 2005. Times–dates are plotted the same as in Fig. 5. The distance scale in (a) and the color bar beside (h) provide references of scale and reflectivity values for each image, and the location of the radar is indicated by a cyan cross. (Images are available online at http://www.srh.noaa.gov/mfl/katrina.)

TABLE 2. Selected best-track information for storms included in the analog climatology.

Storm name	Yr	Start date	End date	Max intensity ($m\ s^{-1}$)
Andrew	1992	1800 UTC 16 Aug	0600 UTC 28 Aug	77
Betsy	1965	0000 UTC 27 Aug	0000 UTC 13 Sep	69
Dawn	1972	0000 UTC 5 Sep	1200 UTC 14 Sep	36
Harvey	1999	0600 UTC 19 Sep	0000 UTC 22 Sep	26
How	1951	0600 UTC 28 Sep	1200 UTC 8 Oct	48
Isbell	1964	1200 UTC 8 Oct	0000 UTC 17 Oct	56
Mitch	1998	0000 UTC 22 Oct	1800 UTC 9 Nov	79
Wilma	2005	1800 UTC 15 Oct	1800 UTC 26 Oct	82

for maintaining the PI at levels conducive to continued intensification.

Between 0600 UTC 27 August and 0000 UTC 28 August, near-surface wind speeds around Katrina remain constant near 50 $m\ s^{-1}$; however, the size and symmetric structure of the storm increase dramatically (Figs. 7 and 11d,e). Cold cloud tops cover the eastern half of the Gulf of Mexico by the end of the period (Fig. 11e), the radius of TS-force winds associated with Katrina have doubled (Fig. 7) and the radius of maximum wind has increased to 110 km, its maximum value for Katrina's life cycle (Table 5). Despite the plateau in intensity, the system's total PD (Emanuel 2005) continues to increase monotonically because of Katrina's increasing size (Fig. 14, see section 2 for a description of the PD calculation used in this study). The exponential increase in PD throughout the intensification of Hurricane Katrina suggests that this quantity is physically meaningful and that it has potential applications for analysis and prediction of the episodic rapid intensification periods often observed during hurricane spinup. A broader investigation of PD evolution over hurricane life cycles will form the basis of a future study.

As the outflow (O) from the expanding system organizes, strong nonconservation of θ_{DT} becomes evident in Figs. 8h,i. By 0000 UTC 28 September, a 28 $m\ s^{-1}$ outflow channel is present to the south of the diabatically generated upper-level anticyclone and the westerly flow north of Katrina has advected the environmental anticyclone A eastward (Fig. 8i). This leads to the amplification of trough "U" (Fig. 8) over the Rocky Mountains, a feature that is of primary importance to Katrina's subsequent evolution.

A second period of rapid intensification occurs between 0000 UTC 28 August and 1200 UTC 28 August. Over this 12-h period, the maximum near-surface winds around Katrina increase from 51 to 77 $m\ s^{-1}$ (category 5) as the storm begins to turn northward ahead of developing trough U (Fig. 8j). The onset of this intensification period does not appear to be associated with the center's passage over a significant SST anomaly (Fig. 9b); however, a study of satellite altimetry data by Scharroo et al. (2005) shows that this development coincides with Katrina's movement over a WCR shed by the Loop Current (Fig. 14). The presence of a measured height anomaly of 20–30 cm across Katrina's track suggests that warm ocean temperatures extend over a deep layer. With category-3–5 winds, Katrina is very effective at inducing mixing-generated cold upwellings during its mature stage (e.g., Hazelworth 1968; Shay et al. 2000, among others). The enhanced heat content of the deep WCR compared to surrounding waters—despite their uniformly warm SSTs—appear to play an important role in the final intensification stage of the system.

Shortly before 1200 UTC 28 August, Katrina becomes superintense as the wind speed around the core exceed the PI of 69 $m\ s^{-1}$ by up to 8 $m\ s^{-1}$ (Fig. 10). Persing and Montgomery (2003) use an axisymmetric model to show that the entrainment of high equivalent potential temperature (θ_e) air from the eye into the eyewall is an effective mechanism for producing a superintense hurricane. The results of these experiments are supported by observational evidence gathered during the intense phase of Hurricane Isabel (2003) and studied in detail by Montgomery et al. (2006a). Although a high-resolution θ_e dataset is not currently

TABLE 3. Statistics for data used in the analog climatology study.

Dataset	Members	Mean ($m\ s^{-1}$)	Std dev ($m\ s^{-1}$)
Landfall (sample)	8	−1.0	7.5
Life cycle (population)	38	0.0	13.8

TABLE 4. Statistical results for the TOST equivalence test (Schuirmann 1987).

Interval test	Degrees of freedom	*T*-test result	Significance
Low ($>V_1$)	8	3.23	>95%
High ($<V_2$)	8	2.64	>95%

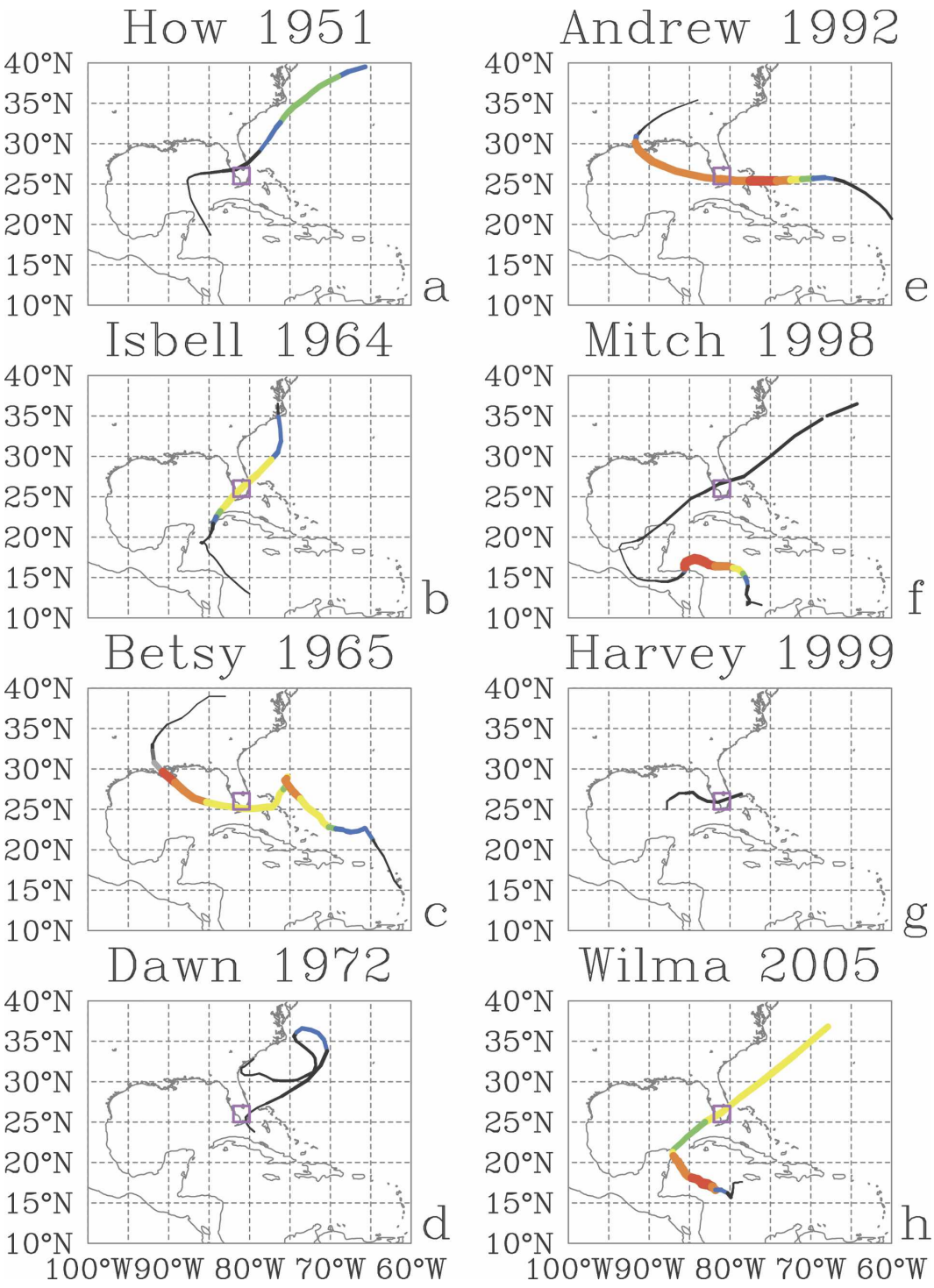

FIG. 13. Track maps for the eight storms matching the analog criteria outlined in section 4b. The width of the track line is directly proportional to the minimum MSLP, and colors correspond to intensity categories: TD (black); category 1 (blue); category 2 (green); category 3 (yellow); category 4 (orange); and category 5 (red). A dashed line indicates a system that has undergone ET and is defined as extratropical by the NHC.

TABLE 5. Radius of Katrina's eye at selected times from 1200 UTC 25 Aug to 0000 UTC 30 Aug 2005, depending on data availability. The observing platforms used to diagnose the eye radius are noted in the final column—NOAA Hurricane Hunter Doppler radar data (N43RF); NOAA (Miami) ground-based Doppler radar (WSR-88D); polarization corrected temperature satellite imagery (PCT); standard infrared satellite imagery (IR); and visible satellite imagery (VIS). Images from both Defense Meteorological Satellite Program's Special Sensor Microwave Imager (SSM/I) and *Aqua* satellites were used in the analysis as noted, depending on the position of the swath at critical times.

Date	Eye radius (km)	Observing platform
1200 UTC 25 Aug	50	N43RF
0000 UTC 26 Aug	50	SSMI (PCT) + WSR-88D
1200 UTC 26 Aug	40	SSMI (PCT) + WSR-88D
0000 UTC 27 Aug	90	SSMI (PCT)
1200 UTC 27 Aug	95	SSMI (IR) + N43RF
0000 UTC 28 Aug	110	SSMI (PCT + IR + VIS)
1200 UTC 28 Aug	85	SSMI (PCT + IR)
1800 UTC 28 Aug	50	N43RF
0000 UTC 29 Aug	50	SSMI (PCT + IR + VIS) + N43RF
1200 UTC 29 Aug	90	*Aqua* (PCT + IR) + N43RF
0000 UTC 30 Aug	35	SSMI (PCT)

available for Katrina's core [one may eventually be developed from data collected during the Rainband and Intensity Change Experiment (RAINEX; see online at http://www.eol.ucar.edu/projects/rainex)], we hypothesize that the depth of the warm layer in the WCR may assist with the elevation of the lower-level θ_e by reducing the effectiveness of wind-induced mixing as noted above.

Upon reaching its peak intensity at 1200 UTC 28 August, Katrina begins to weaken and to accelerate northward. The shear over the center increases to 15 m s^{-1} (Fig. 10) ahead of approaching trough U (Figs. 8j,k). Despite this, the structure of the storm remains symmetric (Fig. 11f) and the outflow anticyclone still possesses well-defined channels with wind speeds exceeding 25 m s^{-1} both equatorward and poleward of the center. As shown in Fig. 14 and Scharroo et al. (2005), Katrina's drop in intensity, most clearly shown by the storm's PD (Fig. 14), coincides with its movement over shelf waters where dynamic topography heights are 20 cm below the baseline. This implies that the available heat energy beneath the system decreases dramatically at the onset of weakening despite consistently high temperatures in the thin surface layer, represented by the SSTs shown in Figs. 9b and 10. Combined with increasing vertical shear, this leads to Katrina's weakening to a category-3 hurricane with maximum near-surface winds of 56 m s^{-1} by the time the storm makes landfall in Buras, Louisiana, at 1110 UTC 29 August.

The subsequent expansion of Katrina's circulation (Table 5 and Fig. 7) early on 29 August is responsible for a secondary peak in the storm's PD (Fig. 14), a quantity closely related to the disaster potential of a TC (Southern 1979). Although the system's PD drops quickly between Buras and Katrina's final landfall on the Louisiana–Mississippi border shortly before 1500 UTC 29 August, it is likely that the devastating effects of the weakening category-3 storm are enhanced by this PD spike in the final stages of its tropical phase.

5. Extratropical transition

Hurricane Katrina's weakening trend that began 23 h before landfall (section 4c) accelerates as the storm moves over land (Fig. 10). By 0000 UTC 30 August, westerly DT winds of up to 45 m s^{-1} form between Katrina's outflow anticyclone (O) and the cooler air to its north and west (Fig. 8m). This steering flow triggers the recurvature of the system by 1200 UTC 30 August (Fig. 1) as the storm begins to accelerate northeastward. The increasing forward speed results in the development of marked asymmetries in Katrina's lower-level wind field as the region of TS-force winds expands to the right of the track in accordance with the gradient wind balance (Fig. 7). The northward advection of warm, moist tropical air associated with Katrina's local environment strengthens a preexisting northeast–southwest-oriented baroclinic zone over the eastern

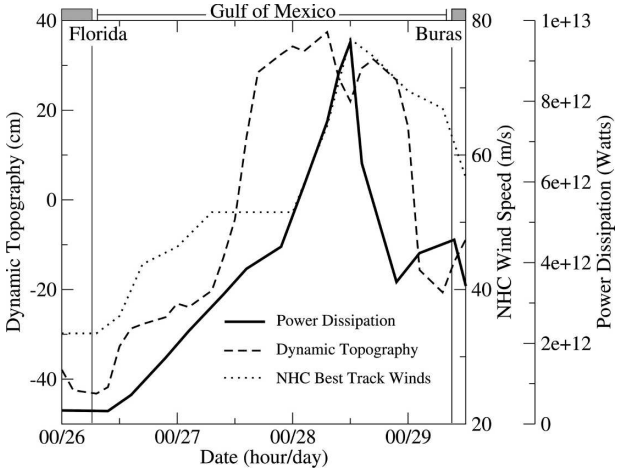

FIG. 14. Power dissipation (heavy solid line), satellite-derived dynamic topography (heavy dashed line), and best-track wind speeds (dotted line) for Hurricane Katrina from 0000 UTC 26 Aug to 1200 UTC 29 Aug 2005. Section 2 contains a description of the method used to compute the PD.

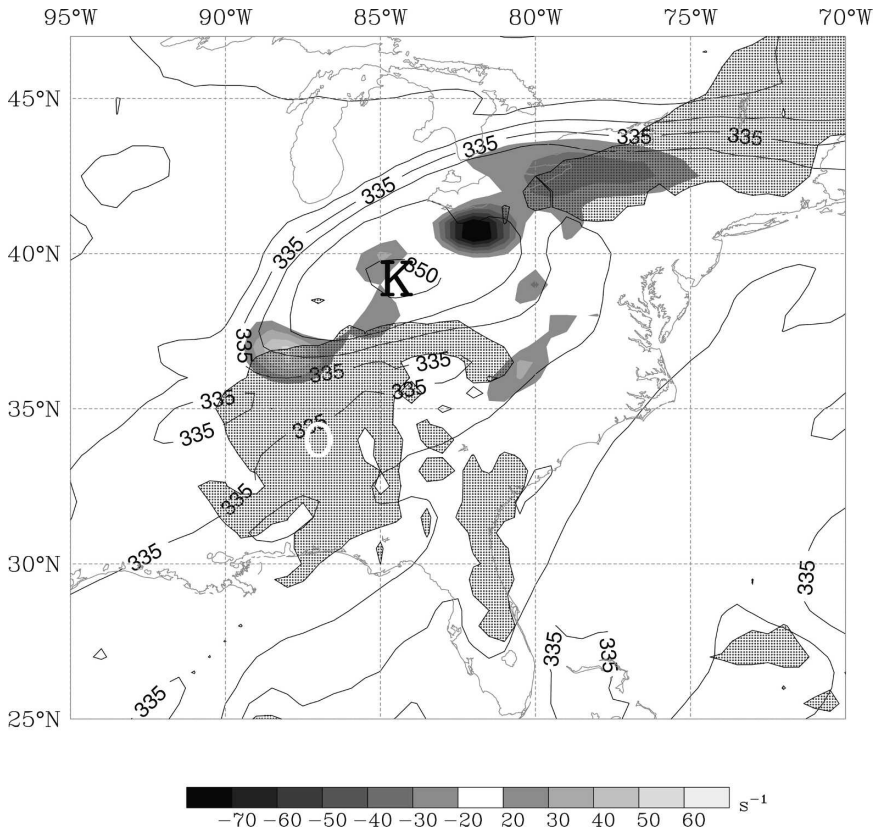

FIG. 15. Equivalent potential temperature at 500 hPa (contoured at 5-K intervals), satellite brightness temperature as shown in Fig. 11 (threshold shading below 260 K), and 850–500-hPa mean moisture convergence (s^{-1}, shading as indicated on the grayscale bar) for 0000 UTC 31 Aug 2005. Annotations follow the text and are summarized in Table 1.

United States (not shown) and isentropic ascent leads to the development of deep clouds and precipitation over the northeastern states and southeastern Canadian provinces on 30 and 31 August (Figs. 11g,h and 15).

The strong westerly upper-level flow induced by approaching trough U advects Katrina's outflow anticyclone (O) eastward on 30 August, exposing the lower-level circulation to the strong shears and cooler upper-level air associated with the trough (Fig. 8n). The rapid evolution of the system is noticeable in Fig. 15, where the midlevel warm core (labeled "K" as the remnant of Katrina's cyclonic circulation) is located over 5° to the north-northwest of the upper-level cloud shield. This ET process is characterized by the forceful removal of the deep warm core by a strong upper-level flow rather than the more typical baroclinic evolution of the midlatitude feature in conjunction with a lower-level vorticity maximum and increased local temperature gradients (Jones et al. 2003). As shown in Fig. 16, the transition of Katrina from symmetric warm core to asymmetric cold core occurs virtually instantaneously just before 1200 UTC 30 August (Hart 2003).

The lower-level remnant of Katrina continues to track northeastward until 1200 UTC 1 September, at which time further interaction with a stationary low over James Bay causes it to meander northward (Fig. 1). Despite a slight (10 hPa) reduction in the minimum MSLP of the system on 2 September, wind speeds around the remnant remain low. Katrina's life cycle ends on 7 September when the final traces of the storm's lower-level circulation are absorbed by an extratropical system near the southern tip of Greenland. Therefore, despite Katrina's remarkable intensity and PD as a hurricane, the system dissipates following ET.

Despite Katrina's failure to reintensify following ET, an important component of the former TC's structure continues to influence the flow over the eastern United States into early September. Katrina's outflow anticyclone (O), sheared eastward by strong winds ahead of trough U between 30 August and 1 September, remains close to the eastern seaboard and continues to interact with the upstream trough (Figs. 8m–p). This trough–ridge couplet, a direct result of the strong latent heating in the TC, establishes an anomalous southerly flow

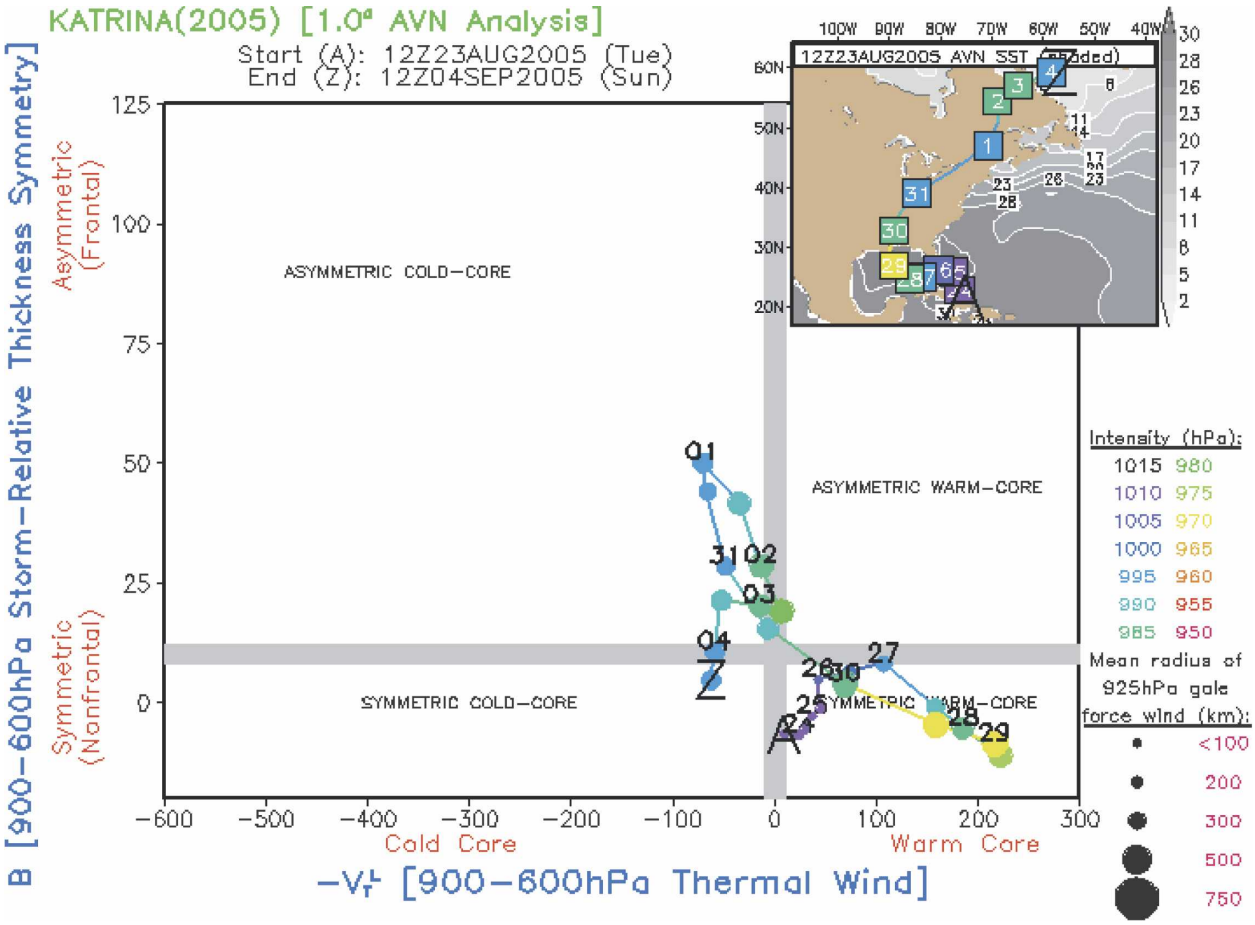

FIG. 16. Cyclone phase space (Hart 2003) representation of Hurricane Katrina's life cycle. The thermal asymmetry of the system (ordinate) is plotted against the lower-level thermal wind (abscissa) at 12-hourly intervals from the 1° GFS analysis with dot sizes corresponding to the gale-force wind radius at 925 hPa and colors chosen according to minimum MSLP. Hurricane Katrina starts at point A in the phase space and finishes at point Z, moving along the geographical track shown in the inset. (Figure courtesy of R. Hart.)

component over eastern North America through late August and early September (Fig. 17). This pattern will result in the northward transport of features entering the "conduit" from the southwestern United States and northern Mexico. Part II will describe how this anomalous connection between the Tropics and the midlatitudes has a notable impact on the hemispheric flow over a period of nearly 2 weeks.

6. Summary and discussion

The landfalls of Hurricane Katrina in Florida and Louisiana left a swath of devastation whose cost in lives and dollars exceeds any other U.S. natural disaster in living memory. This study focused on a diagnosis of the complete life cycle of Katrina, from the storm's development as a TT to its eventual dissipation as an ET. Such a study is necessary because of the magnitude of the disaster that Katrina caused and because of the possibility that an overall upswing in North Atlantic hurricane activity (either naturally cyclic or forced by climate change) could result in an increased frequency of similar threats to fragile coastal infrastructure in the future.

The primary precursors for Katrina's development have been shown to be the remnant lower- to midlevel circulation from TD 10 and a PV tail of midlatitude origin that remained nearly stationary over the eastern Caribbean for a period of 1 week before Katrina's genesis. As the TD-10 vortex moved through a region of quasigeostrophically forced enhanced convection downshear of the trough, it focused diabatic forcing along its track. Just 24 h later, an initially dry easterly wave provided further cyclogenetic forcing in the area. This second period of organization gave rise to an incipient lower-level circulation that began to intensify and evolved into Katrina.

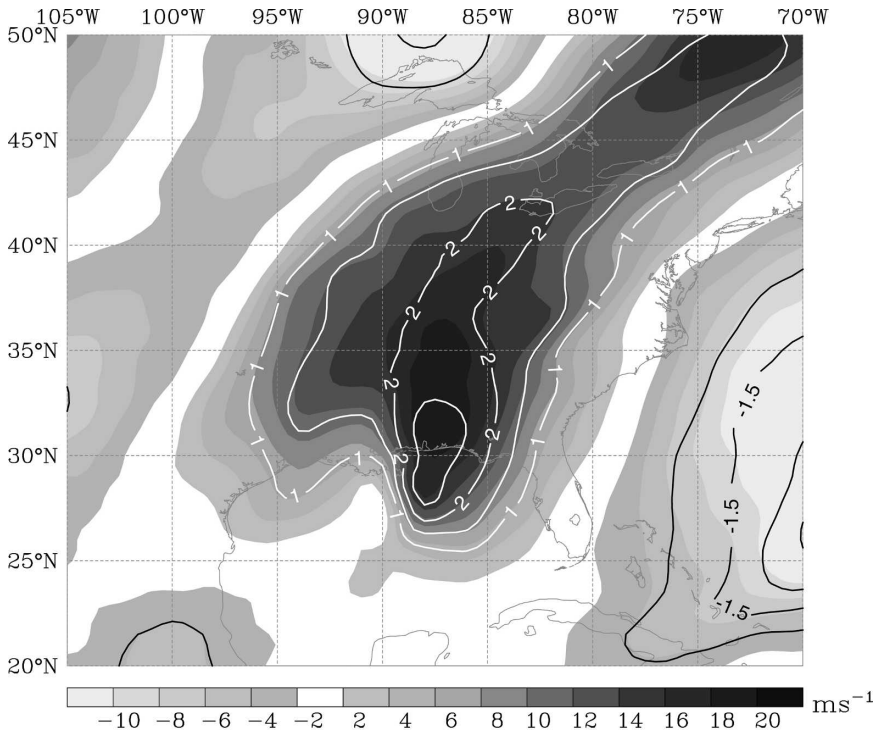

FIG. 17. Mean 200–300-hPa meridional winds (m s^{-1}) between 0000 UTC 29 Aug and 0000 UTC 1 Sep 2005 (shading as indicated on the grayscale bar with positive values for southerly winds), and the corresponding fractional anomaly values normalized by the zonal standard deviation (solid contours at 0.5 standard deviation increments, white for southerly winds and black for northerly winds). For example, a normalized anomaly value of +2.0 indicates that the southerly wind is two standard deviations greater than the zonal average at the location of interest.

Steered through a weak shear environment east of Florida by flow associated with a θ_{DT} maximum over the U.S. Gulf coast, Katrina crossed the warm Gulf Stream waters—a region associated with elevated PI values—and reached category-1 status just before making landfall near Miami, Florida. An analog climatological study was used to show that Katrina's maintenance of intensity during its crossing of the Florida peninsula was consistent with the historical record. This finding suggests that landfall on the southern peninsula should not be considered a harbinger of significant perturbations to the intensity of TCs.

Two periods of rapid intensification in the Gulf of Mexico brought Katrina to category-5 strength while the 18-h quiescent period between these stages was accompanied by a doubling in the storm's size. The PD of Katrina was shown to increase monotonically over time until the storm reached a superintense state on 28 August—with respect to the Bister and Emanuel (1997) PI—and began to weaken. Given the uniformly warm SSTs in the Gulf of Mexico over the period, this continuous increase in storm energy may be a significant result worthy of further study. Satellite altimetry data were used to show that Katrina's final intensification stage coincided with the storm's passage over a deep WCR that may have reduced the mixing of cooler waters to the surface beneath the hurricane.

Immediately after leaving the WCR, Katrina began to weaken, dropping to category-3 strength before making its final devastating landfalls in Louisiana. Interaction with an upstream trough initiated a rapid ET process shortly after landfall, as Katrina's outflow anticyclone was sheared rapidly eastward by strong westerlies ahead of the trough. This led to a replacement of the deep warm core structure of the TC with cold air aloft in a time frame of less than 6 h. The lower-level remnants of Katrina failed to reintensify but Katrina's outflow anticyclone remained over the western North Atlantic and continued to interact with the upstream trough for several days following ET. This pattern es-

tablished an anomalous southerly component in the flow over eastern North America that will be investigated in detail in Part II.

The findings of this diagnostic study have potential impact on the forecasting of future TCs that form near the North American continent and intensify rapidly in the Gulf of Mexico. An understanding of the TT process in the western equatorial Atlantic, the effect of a Florida landfall on a hurricane's evolution, the exponential increase in PD, the influence of sea surface and deep-layer ocean temperatures, and the interaction of the TC's outflow with the environment during ET is crucial to the overall picture of Hurricane Katrina's complex evolution. An enhanced appreciation for each of these important life cycle components may have a positive impact on our ability to predict, and hopefully prevent, future TC-related disasters of this magnitude.

Acknowledgments. The authors thank Robert Hart for providing the CPS figure for Hurricane Katrina and Remko Scharroo for processing and providing the satellite altimetry data for this study. This work was supported by NSF Grant ATM0304254, the Canadian Foundation for Climate and Atmospheric Sciences, and the Canadian Natural Sciences and Engineering Research Council.

REFERENCES

Abraham, J., J. W. Strapp, C. Fogarty, and M. Wolde, 2004: Extratropical transition of Hurricane Michael: An aircraft investigation. *Bull. Amer. Meteor. Soc.,* **85,** 1323–1339.

Anwender, D., M. Leutbecher, S. C. Jones, and P. A. Harr, 2006: Sensitivity of ensemble forecasts of extratropical transition to initial perturbations targeted on the tropical cyclone. Preprints, *27th Conf. on Hurricanes and Tropical Meteorology,* Monterey, CA, Amer. Meteor. Soc., 4A.5.

Atallah, E. H., and L. F. Bosart, 2003: The extratropical transition and precipitation distribution of Hurricane Floyd 1999. *Mon. Wea. Rev.,* **131,** 1063–1081.

——, ——, and A. R. Aiyyer, 2007: Precipitation distribution associated with landfalling tropical cyclones over the eastern United States. *Mon. Wea. Rev.,* **135,** 2185–2206.

Bell, G. D., and M. Chelliah, 2006: Leading tropical modes associated with interannual and multidecadal fluctuations in North Atlantic hurricane activity. *J. Climate,* **19,** 590–612.

Bender, M. A., I. Ginnis, and Y. Kurihara, 1993: Numerical simulations of tropical cyclone-ocean interaction with a high resolution coupled model. *J. Geophys. Res.,* **98,** 23 245–23 263.

Bergeron, T., 1954: The problem of tropical hurricanes. *Quart. J. Roy. Meteor. Soc.,* **80,** 131–164.

Bister, M., and K. A. Emanuel, 1997: The genesis of Hurricane Guillermo: TEXMEX analyses and a modeling study. *Mon. Wea. Rev.,* **125,** 2662–2682.

Bosart, L. F., and F. Sanders, 1981: The Johnstown Flood of July 1977: A long-lived convective system. *J. Atmos. Sci.,* **38,** 1616–1642.

——, and J. A. Bartlo, 1991: Tropical storm formation in a baroclinic environment. *Mon. Wea. Rev.,* **119,** 1979–2013.

——, C. S. Velden, E. W. Bracken, J. Molinari, and P. G. Black, 2000: Environmental influences on the rapid intensification of Hurricane Opal 1995: Over the Gulf of Mexico. *Mon. Wea. Rev.,* **128,** 322–352.

Bracken, W. E., and L. F. Bosart, 2000: The role of synoptic-scale flow during tropical cyclogenesis over the North Atlantic Ocean. *Mon. Wea. Rev.,* **128,** 353–376.

Churney, B., 2006: Underwriting catastrophe risk: Post Hurricane Katrina. *J. Reinsurance,* **13,** 1–14.

Colle, B. A., 2003: Numerical simulation of the extratropical transition of Floyd 1999: Structural evolution and responsible mechanisms for the heavy rainfall over the northeastern United States. *Mon. Wea. Rev.,* **131,** 2905–2926.

Davis, C., and L. F. Bosart, 2004: The TT problem. *Bull. Amer. Meteor. Soc.,* **85,** 1657–1662.

DeMaria, M., 1996: The effect of vertical shear on tropical cyclone intensity change. *J. Atmos. Sci.,* **53,** 2076–2088.

Eady, E., 1949: Long waves and cyclone waves. *Tellus,* **1,** 33–52.

Emanuel, K. A., 1987: An air-sea interaction model of intraseasonal oscillations in the Tropics. *J. Atmos. Sci.,* **44,** 2324–2340.

——, 2005: Increasing destructiveness of tropical cyclones over the past 30 years. *Nature,* **426,** 686–688.

Ferreira, R. N., and W. H. Schubert, 1999: The role of tropical cyclones in the formation of tropical upper-tropospheric troughs. *J. Atmos. Sci.,* **56,** 2891–2907.

Goldenberg, S. B., C. W. Landsea, A. M. Mestas-Nunez, and W. M. Gray, 2001: The recent increase in Atlantic hurricane activity: Causes and implications. *Science,* **293,** 474–479.

Gray, W., 1968: Global view of the origin of tropical disturbances and storms. *Mon. Wea. Rev.,* **96,** 669–700.

Hanley, D. E., J. Molinari, and D. Keyser, 2001: A composite study of the interactions between tropical cyclones and upper-tropospheric troughs. *Mon. Wea. Rev.,* **129,** 2570–2584.

Harr, P. A., D. Anwender, and S. C. Jones, 2006: Predictability associated with the downstream impacts of the extratropical transition (ET) of tropical cyclones. Preprints, *27th Conf. on Hurricanes and Tropical Meteorology,* Monterey, CA, Amer. Meteor. Soc., P6.7.

Hart, R. E., 2003: A cyclone phase space derived from thermal wind and thermal asymmetry. *Mon. Wea. Rev.,* **131,** 585–616.

——, and J. L. Evans, 2001: A climatology of the extratropical transition of Atlantic tropical cyclones. *J. Climate,* **14,** 546–564.

Hazelworth, J. B., 1968: Water temperature variations resulting from hurricanes. *J. Geophys. Res.,* **73,** 5105–5123.

Hoskins, B., M. McIntyre, and A. Robertson, 1985: On the use and significance of isentropic potential vorticity maps. *Quart. J. Roy. Meteor. Soc.,* **111,** 877–946.

Hubert, L. F., 1955: Frictional filling of hurricanes. *Bull. Amer. Meteor. Soc.,* **36,** 440–445.

Jones, S. C., and Coauthors, 2003: The extratropical transition of tropical cyclones: Forecast challenges, current understanding, and future directions. *Wea. Forecasting,* **18,** 1052–1092.

Knabb, R. D., J. R. Rhome, and D. P. Brown, 2005: Tropical cyclone report: Hurricane Katrina (23–30 August 2005). Tech. Rep., National Hurricane Center, National Oceanographic and Atmospheric Administration, 43 pp. [Available online at http://www.nhc.noaa.gov/pdf/TCR-AL122005_Katrina.pdf.]

McTaggart-Cowan, R., J. R. Gyakum, and M. K. Yau, 2003: The influence of the downstream state on extratropical transition:

Hurricane Earl (1998) case study. *Mon. Wea. Rev.,* **131,** 1910–1929.

——, L. F. Bosart, J. R. Gyakum, and E. H. Atallah, 2007: Hurricane Katrina (2005). Part II: Evolution and hemispheric impacts of a diabatically generated warm pool. *Mon. Wea. Rev.,* **135,** 3927–3949.

Miller, B. I., 1964: A study of the filling of Hurricane Donna 1960: Over land. *Mon. Wea. Rev.,* **92,** 389–406.

Molinari, J., D. Vollaro, and K. Corbosiero, 2004: Tropical storm formation in a sheared environment. *J. Atmos. Sci.,* **61,** 2493–2509.

Montgomery, M. T., M. M. Bell, S. D. Aberson, and M. L. Black, 2006a: Hurricane Isabel (2003): New insights into the physics of intense storms. Part I: Mean vortex structure and maximum intensity estimates. *Bull. Amer. Meteor. Soc.,* **87,** 1335–1347.

——, M. E. Nicholls, T. A. Cram, and A. B. Saunders, 2006b: A vortical hot tower route to tropical cyclogenesis. *J. Atmos. Sci.,* **63,** 355–386.

Persing, J., and M. T. Montgomery, 2003: Hurricane superintensity. *J. Atmos. Sci.,* **60,** 2349–2371.

Powell, M. D., P. J. Vickery, and T. A. Reinhold, 2003: Reduced drag coefficients for high wind speeds in tropical cyclones. *Nature,* **422,** 279–283.

Powers, J. G., and C. A. Davis, 2002: A cloud-resolving regional simulation of tropical cyclone formation. *Atmos. Sci. Lett.,* **3,** 15–24.

Sadler, J. C., 1976: A role of the tropical upper tropospheric trough in early season typhoon development. *Mon. Wea. Rev.,* **104,** 1266–1278.

——, 1978: Mid-season typhoon development and intensity change and the tropical upper tropospheric trough. *Mon. Wea. Rev.,* **106,** 1137–1152.

Scharroo, R., W. H. F. Smith, and J. L. Lillibridge, 2005: Satellite altimetry and the intensification of Hurricane Katrina. *Eos, Trans. Amer. Geophys. Union,* **86,** 366–367.

Schuirmann, D. J., 1987: A comparison of the two one-sided tests procedure and the power approach for assessing the equivalence of average biodiversity. *J. Pharmacokinet. Biopharm.,* **15,** 657–680.

Shay, L. K., G. J. Goni, and P. G. Black, 2000: Effects of a warm oceanic feature on Hurricane Opal. *Mon. Wea. Rev.,* **128,** 1366–1383.

Simpson, J., E. Ritchie, J. Holland, J. Halverson, and S. Stewart, 1997: Mesoscale interactions in tropical cyclone genesis. *Mon. Wea. Rev.,* **125,** 2643–2661.

Simpson, R. H., 1974: The hurricane disaster potential scale. *Weatherwise,* **27,** 169–186.

Southern, R. L., 1979: The global socio-economic impact of tropical cyclones. *Aust. Meteor. Mag.,* **27,** 175–195.

Zehr, R. M., 1992: Tropical cyclogenesis in the western North Pacific. Tech. Rep. NESDIS 61, NOAA Tech. Rep., NOAA/National Environmental Satellite, Data, and Information Service, Washington, DC, 181 pp.

Zurita, P., and R. S. Lindzen, 2001: The equilibration of short Charney waves: Implications for potential vorticity homogenization in the extratropical troposphere. *J. Atmos. Sci.,* **58,** 3443–3462.